DOI: 10.1002/chem.200700382

Electron Transfer to Sulfides and Disulfides: Intrinsic Barriers and Relationship between Heterogeneous and Homogeneous Electron-Transfer Kinetics

Ana Belèn Meneses,[a, b] Sabrina Antonello,[a] Maria Carmen Arévalo,*[b] Concepcion Carmen González,[c] Jadab Sharma,[a] Andrea N. Wallette,[d] Mark S. Workentin,*[d] and Flavio Maran*[a]

In memory of Professor Sergio Roffia

Abstract: The electron-acceptor properties of series of related sulfides and disulfides were investigated in *N*,*N*-dimethylformamide with homogeneous (redox catalysis) and/or heterogeneous (cyclic voltammetry and convolution analysis) electrochemical techniques. The electron-transfer rate constants were determined as a function of the reaction free energy and the corresponding intrinsic barriers were determined. The dependence of relevant thermodynamic and kinetic parameters on substituents was assessed. The kinetic data were also analyzed in relation to corresponding data pertaining to reduction of diaryl disulfides. All investigated reductions take place by stepwise dissociative electron transfer (DET) which causes cleavage of the C_{alkyl}–S or S–S bond. A generalized picture of how the intrinsic electron-transfer barrier depends on molecular features, ring substituents, and the presence of spacers between the frangible bond and aromatic groups was established. The reduction mechanism was found to undergo a progressive (and now predictable) transition between common stepwise DET and DET proceeding through formation of loose radical anions. The intrinsic barriers were compared with available results for ET to several classes of dissociative- and nondissociative-type acceptors, and this led to verification that the heterogeneous and the homogeneous data correlate as predicted by the Hush theory.

Keywords: electrochemistry · electron transfer · reduction · substituent effects · sulfur

[a] A. B. Meneses, Dr. S. Antonello, Dr. J. Sharma, Prof. Dr. F. Maran
Dipartimento di Scienze Chimiche
Università di Padova
Via Marzolo 1, 35131 Padova (Italy)
Fax (+39) 049-827-5239
E-mail: flavio.maran@unipd.it

[b] A. B. Meneses, Prof. Dr. M. C. Arévalo
Departamento de Química Fisíca
Universidad de la Laguna
Avda. Astrofísico Fco Sánchez s/n, 38071 La Laguna (Spain)
Fax: (+34) 922-318-002
E-mail: carevalo@ull.es

[c] Dr. C. C. González
Instituto de Productos Naturales y Agrobiologia del CSIC
Universidad de la Laguna
Avda. Astrofísico Fco Sánchez s/n, 38071 La Laguna (Spain)

[d] A. N. Wallette, Prof. Dr. M. S. Workentin
Department of Chemistry
The University of Western Ontario
N6A 5B7 London, Ontario (Canada)
Fax: (+1) 519-661-3022
E-mail: mworkent@uwo.ca

Supporting information for this article is available on the WWW under http://www.chemeurj.org/ or from the author.

Introduction

During the last two decades, substantial knowledge of the thermodynamics, kinetics, and mechanisms of electron-transfer (ET) reactions associated with cleavage of a σ bond (dissociative ET, DET) has been accumulated. Several aspects of reductive DET, particularly with regard to carbon–halogen and O–O bonds, have been investigated and reviewed.[1–3] Dissociative reduction of a neutral species A–B to form a radical A$^{\bullet}$ and an anion B$^-$ may proceed either through formation of a discrete radical anion intermediate A–B$^{\bullet-}$ [stepwise DET, Eq. (1)] or concertedly [Eq. (2)].

$$A{-}B + e \rightleftharpoons A{-}B^{\bullet-} \rightarrow A^{\bullet} + B^- \quad (1)$$

$$A{-}B + e \rightarrow A^{\bullet} + B^- \quad (2)$$

The reaction pathway followed by the reduction is a function of parameters that may be directly associated with the acceptor molecule, such as the nature of the cleaving bond, the properties of substituents, and the redox potential of the

leaving group, or externally driven, such as temperature, solvent, and the electrode potential (for heterogeneous reductions) or the standard potential of the solution one-electron donor (for homogeneous reductions). In fact, it has been found that even for a single acceptor molecule, the DET mechanism can be changed by modifying one or more of such parameters.[4–7] The transition between the two limiting mechanisms of thermal DET can be detected by using homogeneous redox catalysis[8] or direct electrochemical methods,[4c] and these approaches have been thoroughly analyzed and discussed.

An important factor that differs between the ET steps of the two mechanisms is the intrinsic barrier $\Delta G_0^{\neq}$,[9] that is, the activation free energy $\Delta G^{\neq}$ when the reaction free energy ($\Delta G°$) is 0, which characterizes the kinetic facility of the ET reaction. The $\Delta G_0^{\neq}$ value is composed of an outer component, namely, the solvent reorganization energy ($\Delta G_{0,s}^{\neq}$), and an inner component ($\Delta G_{0,i}^{\neq}$), which describes the molecular deformation (of bond lengths and bond angles) of the reacting system.[9] The $\Delta G_{0,s}^{\neq}$ is the most important factor determining the kinetics of ET proceeding through the formation of rigid transient radical anions, where reduction causes little molecular deformation and the singly occupied molecular orbital (SOMO) is very weakly coupled to the σ* orbital of the cleaving bond; this behavior is typical of most ethers and aryl halides.[1,3] In this mechanism, the bond-cleavage step is an intramolecular DET from the π* SOMO to the A–B σ* orbital. The cleavage step is accompanied by stretching of the A–B bond and significant solvent reorganization (as the charge is eventually localized on the leaving group). In the limiting case of concerted DETs, $\Delta G_0^{\neq}$ is much larger because the inner reorganization contains as much as one-fourth of the dissociation energy of the cleaving bond[10] and is thus much larger than the $\Delta G_{0,s}^{\neq}$ term.

The recent observation of the occurrence of borderline mechanisms makes the distinction between the two DET reactions less straightforward.[1b,2] There are stepwise processes in which the initial ET has a significant inner reorganization energy. This happens when the SOMO involves the frangible bond, whereby the A–B bond length (the A–B bond order decreases), and thus $\Delta G_{0,i}^{\neq}$ increases. For some compounds, such as most disulfides,[11,12] the SOMO is more localized on the S–S bond so that it essentially corresponds to the σ* orbital. The ET intermediate now is a loose σ* radical anion, as opposed to the more rigid framework of the π* radical anions that form in common stepwise DET processes. The $\Delta G_0^{\neq}$ for formation of the loose radical anion is thus quite large, but still not as large as that of concerted DET. Concerted DET reactions can form caged fragmentation products that can undergo ion–dipole interactions, in which the anionic leaving group, B–, electrostatically interacts with the dipole moment present in the radical fragment A•.[2,3] In concerted DETs, the A–B bond length is an important component of the reaction coordinate. In the case of ion–dipole interactions, this A–B bond elongation is less pronounced, the resulting transition state becomes more reactantlike, and the activation energy decreases accordingly. The $\Delta G_0^{\neq}$ value can become significantly smaller than that of uncomplicated concerted dissociative processes and thus its magnitude may be comparable to that of the loose radical anion DET mechanism. Clear-cut examples of this borderline DET mechanism are provided by the reduction of substituted benzyl halides[13] and halo acetonitriles.[14]

Because of specific features of the acceptor molecule and, to some extent, the dielectric and molecular properties of the solvent, different DET mechanisms may occur whose detection requires determination of relevant parameters, particularly the $\Delta G_0^{\neq}$ value. Among the various classes of DET acceptor molecules, an unifying understanding of the reductive cleavage of the C–S bond of sulfides is still lacking. This is partly because these DET reactions appear to be particularly suited to give rise to mixed mechanistic behaviors, as already observed and/or discussed.[1,4a,15,16] For example, certain sulfides are reduced with substantial inner reorganization caused by C–S bond elongation on radical-anion formation.[15c,d] In one case, some evidence for a concerted-to-stepwise mechanistic transition induced by driving force was obtained by studying the dissociative reduction of triphenylmethyl phenyl sulfide by a series of solution one-electron donors,[4a] though a different selection of mediators did not reveal the same activation/driving force trend.[16] Concerning disulfides, more qualitative and quantitative information is available,[11,12] but factors remain that are unexplored. Understanding the reductive cleavage of C–S and S–S bonds in terms of both their kinetics and thermodynamics is essential to improve our knowledge of important organic and biological systems.[17] In particular, a main goal of current research in the field is to establish a sufficiently accurate model to predict the reactivity of these bonds toward electron uptake in complex systems such as proteins and polymer networks.

To systematically address the issue of understanding how different molecular features affect the ET step and the cleavage dynamics, the dissociative reduction of series of related acceptors is studied by using direct (heterogeneous DET) and/or indirect (homogeneous DET) electrochemical methods.[1–3] Here we describe the dynamics of radical-anion formation in the reduction of series of diphenylmethyl *para*-substituted phenyl sulfides Ph_2CHSAr (**1**), triphenylmethyl *para*-substituted phenyl sulfides Ph_3CSAr (**2**), and symmetrical *para*- or *meta*-substituted benzyl disulfides, $(ArCH_2S)_2$ (**3**); for comparison, direct reduction of the disulfide of diphenylethanethiol $(PhCH_2CH_2S)_2$ (**4**), in which the cleaving bond is farther from the aryl groups, was also studied (Table 1). The DET reactions were studied in *N*,*N*-dimethylformamide (DMF) containing tetrabutylammonium perchlorate (TBAP) by using a combination of homogeneous (redox catalysis) and/or heterogeneous (cyclic voltammetry and convolution analysis) approaches. The ET standard rate constants and intrinsic barriers were determined, and the dependence of the relevant thermodynamic and kinetic parameters on substituents assessed. The data were analyzed by using information previously obtained for the reduction

Table 1. Identification of substituents X of **1**–**3** and **5** by labels **a**–**i** (ordered according to their Hammett σ values).

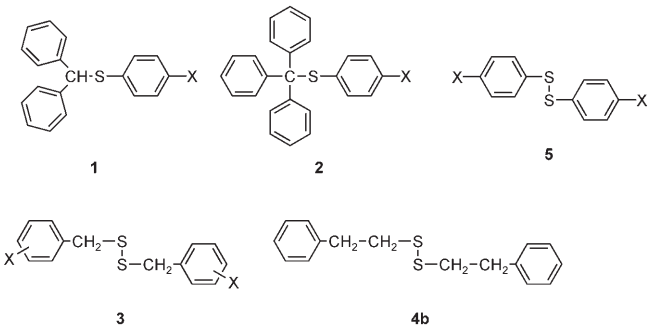

	p-MeO (**a**)	H (**b**)	*p*-F (**c**)	*p*-Cl (**d**)	*p*-CO_2Et (**d**)	*p*-COMe (**f**)	*m*-CN (**g**)	*p*-CN (**h**)	*p*-NO_2 (**i**)
σ	−0.27	0	0.06	0.23	0.45	0.50	0.56	066	0.78
1	+	+	+	+				+	+
2	+	+		+		+		+	+
3	+	+		+			+	+	+
4	+	+	+	+	+			+	+

of diaryl disulfides **5**,[11] which led to a consistent picture of how molecular features (in different classes of compound) and substitution (within the same family of compounds) affect the ET step, particularly its inner barrier, and cause the mechanism to undergo a progressive transition between common stepwise DET and DET proceeding through formation of loose radical anions. Finally, the intrinsic barriers determined were compared with similar data for a variety of other ET and DET acceptors. Thus, it was established for the first time for such a range of compounds that the correlation between the heterogeneous and the homogeneous $\Delta G_0^{\neq}$ values agrees very well with the Hush model.[18]

Experimental Section

Chemicals: DMF (Acros Organics, 99%) was treated with anhydrous Na_2CO_3 and doubly distilled at reduced pressure under a nitrogen atmosphere. Tetra-*n*-butylammonium perchlorate (TBAP, 99%, Fluka) was recrystallized from ethanol/water (2/1) and dried at 60°C under vacuum. The ET mediators were commercially available, except for methyl 3-phenoxybenzoate and phthaloyl-α-aminoisobutyric acid methyl ester, which were available from previous studies.[4d,19]

Sulfides **1** and **2** were synthesized from the appropriate thiophenol and diphenylmethanol or triphenylmethanol in acetic acid with H_2SO_4, and recrystallized from ethanol.[4a,15c,16,20] Dibenzyl disulfides **3** were prepared by the following steps: reaction of the appropriate benzyl bromide with potassium acetate to yield an acetylsulfanyl methylbenzene derivative, transformation of the latter into the thiol under acidic conditions, and oxidation of the thiol to the disulfide with iodine. Full details of the syntheses of sulfide **1h** and disulfides **3** are provided in the Supporting Information. The synthesis of disulfide **4h** will be described elsewhere.

Electrochemistry: For the electrochemical experiments, an EG&G-PARC 173/179 potentiostat/digital coulometer, an EG&G-PARC 175 universal programmer, and a Nicolet 3091 digital oscilloscope with 12-bit resolution were used. The electrochemical experiments were conducted under an Ar atmosphere in an all-glass cell that was thermostated at 25°C. The experiments were carried out inside a double-wall copper Faraday cage. The cage and all instruments were connected to a common ground. To minimize the ohmic drop between the working and reference electrodes, feedback correction was employed.

The electrochemical experiments were performed by using homemade glassy carbon (GC, Tokai GC-20) electrodes 1 mm in diameter that were prepared as previously reported.[21] The GC electrodes were stored in ethanol and were polished before experiments with a 0.25 μm diamond paste (Struers) and ultrasonically rinsed with ethanol for 5 min. The electrodes were electrochemically activated in the background solution by means of several voltammetric cycles at 0.5 $V s^{-1}$ between the anodic and cathodic solvent/electrolyte discharges, until the quality features described in reference [22] were obtained. The electrode area was determined by measuring the limiting convoluted current of ferrocene, whose diffusion coefficient in DMF is 1.13×10^{-5} $cm^2 s^{-1}$.[23] The Ag/AgCl or Ag/AgI reference electrode was calibrated at the end of each experiment against the ferrocene/ferricenium couple, whose formal potential is 0.464 V against the KCl saturated calomel electrode (SCE); in the following, all potentials are reported against SCE. A platinum ring or plate served as the counterelectrode.

The behavior of the working electrode was first studied in the background solution, in a selected potential range, and for scan rates ranging from 0.1 to 100 $V s^{-1}$. The same procedure was repeated after addition of the electroactive species; another series of CVs was acquired after addition of 1 equiv of a weak acid (depending on the type of acceptor: acetic acid, phenol, acetanilide, or trifluoroethanol). For the redox catalysis experiments (which, given the range of ET rate constants investigated, were carried out by CV), the latter procedure was repeated after addition of increasing amounts of the acceptor (twice). A corresponding amount of a weak acid (acetanilide) was always present in solution. Convolution analysis was carried out on digitalized (1 point per mV) background-subtracted CV curves by using our own laboratory software and all necessary precautions required to minimize the electrical noise.[21] To double check the heterogeneous or homogeneous parameters obtained by convolution or redox catalysis, the experimental CV curves were also digitally simulated with the DigiSim 3.03 package by using a step size of 1 mV and an exponential expansion factor of 0.5. The reproducibility of the homogeneous (single donor/acceptor system) and heterogeneous kinetic data (k determination at any investigated E value, as obtained from different experiments and scan rates) was in the range of 5–15%.

Results and Discussion

Direct reduction of sulfides 1: The cyclic voltammograms of sulfides **1a–d** in DMF/0.1 M TBAP display single irreversible peaks at very negative potentials, as previously reported for **1a**[15d] and **1b**;[15b] for example, at 0.2 $V s^{-1}$ the peak potentials E_p are in the range −2.35 to −2.52 V (Table 2). These peaks are irreversible at all scan rates v investigated and broaden as v increases. The electroreduction of **1h** occurs at a more positive potential (−1.86 V) and exhibits a second reversible peak (Figure 1). The formal potential $E°$ of the latter (half-sum between the cathodic and anodic peak potentials) is −2.44 V. In the v range explored, the first peak of **1h** remains irreversible, that is, the ET step is followed by a fast and irreversible chemical reaction. The reduction peak of **1i** is sharper and located at a much more positive potential (−1.08 V), which corresponds to the typical behavior expected for a nitro derivative. As previously reported,[20c] the peak of **1i** already shows some reversibility (appearance of the corresponding anodic peak) at about 1.5 $V s^{-1}$, that is, the chemical reaction affecting the initially formed ET intermediate roughly occurs on the 0.1 s time-

Table 2. Electrochemical and kinetic parameters for the direct reduction of sulfides **1** in DMF/0.1 M TBAP at 25 °C.

1	E_p[a] [V]	$\Delta E_{p/2}$[a] [mV]	α[b]	$10^6 D$ [$cm^2 s^{-1}$]	$E°$[c] [V]	$\log k^\circ_{het}$[c] [$cm\,s^{-1}$]	$(\Delta G_0^{\neq})_{het}$ [$kcal\,mol^{-1}$]	$(\Delta G_{0,i}^{\neq})_{het}$ [$kcal\,mol^{-1}$]
a[d]	−2.52	95	0.502	7.0	−2.45	−2.80	8.7	5.1
b	−2.47	94	0.507	7.6	−2.39	−2.64	8.5	4.6
c	−2.47	98	0.487	7.7	−2.32	−2.96	8.9	5.0
d	−2.35	92	0.526	6.3	−2.30	−2.66	8.5	5.3
h	−1.87	78	0.612	6.6	−1.94	−1.38	6.7	3.3
i	−1.08	58	0.823	6.5	−1.05	−0.77	5.9	2.6

[a] At 0.2 $V\,s^{-1}$. [b] Measured from $\Delta E_{p/2}$. [c] The experimental uncertainty associated with the parameters obtained at $\alpha = 0.5$ is 20 mV ($E°$) and 0.2 lg units ($\lg k^\circ_{het}$). [d] From ref [15d].

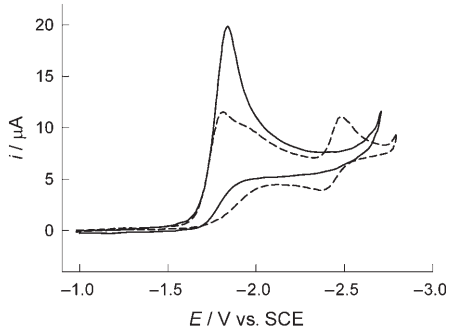

Figure 1. Cyclic voltammetry curves of 5 mM **1h** in DMF/0.1 M TBAP in the absence (dashed line) and presence (solid line) of 1 equiv of acetanilide. GC electrode, 25 °C, 0.02 $V\,s^{-1}$.

scale. As in the case of **1h**, a second reduction peak for **1i** that is reversible even at low scan rate ($E° = -1.52$ V) is observed. Finally, for all sulfides oxidation peaks are detectable during the backward positive-going scan for $E > -0.8$ V; they are associated with oxidation of the carbanionic and/or thiolate species (vide infra) formed in the reduction process.

Previous investigations[15b,d] showed that reduction of this type of sulfide proceeds by cleavage of the C–S bond to form a thiolate ion (ArS^-) and the diphenylmethyl radical ($Ph_2CH^\bullet$); for both thermodynamic (the formal potential $E°$ of $Ph_2CH^\bullet$ is −1.1 V) and kinetic reasons (reduction is accompanied by little reorganization energy),[24] the radical is rapidly reduced to the corresponding carbanion Ph_2CH^-. Since the latter is very basic (the pK_a^{DMF} of Ph_2CH_2 can be estimated to be 32.6)[25a,b] and the original sulfide is the strongest acid in solution (the pK_a^{DMF} of Ph_2CHSPh is 27.2,[25a,c] and that of **1a** was estimated to be only slightly larger;[15d] similarly, the pK_a^{DMF} values of the other sulfides should not be significantly smaller than 27), a self-protonation reaction occurs. By this mechanism,[15b,26] part of the reducible molecule is transformed into its conjugate base and becomes electroinactive at the applied potentials. The overall electron consumption is thus less than the expected two electrons per molecule (if the self-protonation reaction is sufficiently fast, one electron per molecule is consumed).[15b,26] In previous self-protonation studies,[26b] we observed that if the available potential window is sufficiently wide and/or the molecule carries good electron-withdrawing groups, reduction of the conjugate base of the starting molecule can be detected at more negative potentials.

In line with the general behavior of this type of compound, the voltammetric pattern of sulfides **1** is accounted for by the reduction sequence given by [Eqs. (3)–(6)], in which radical anion formation [Eq. (3)] is followed by C–S bond cleavage [Eq. (4)], reduction of $Ph_2CH^\bullet$ [Eq. (5)], and self-protonation [Eq. (6)].

$$Ph_2CHSAr + e \rightleftharpoons Ph_2CHSAr^{\bullet -} \quad (3)$$

$$Ph_2CHSAr^{\bullet -} \rightleftharpoons Ph_2CH^\bullet + ArS^- \quad (4)$$

$$Ph_2CH^\bullet + e \rightarrow Ph_2CH^- \quad (5)$$

$$Ph_2CH^- + Ph_2CHSAr \rightleftharpoons Ph_2CH_2 + Ph_2CSAr^- \quad (6)$$

The reversible second peaks observed in the reduction of **1h** and **1i** are attributed to reduction of the corresponding conjugate base Ph_2CSAr^-. On the positive-going scan, the thiolate anions are oxidized at their characteristic potentials (for the substituents of **1a–i**, the $E°$ values range from −0.07 to 0.53 V)[11b] and so are the carbanions Ph_2CSAr^- (the $E°$ values are in the range −0.7 to −0.8 V). On the other hand, if the water content in the solvent/electrolyte system is not negligible, the latter peak disappears, and this suggests that the self-protonation reaction [Eq. (6)] does not take place (the pK_a^{DMF} of water is 31.7,[25a,d] but H_2O is an OH acid and thus protonation is kinetically faster than with common CH acids). As previously done for **1a** and **1b**,[15b,d] we applied the appropriate theory[15b] and found very similar values of the self-protonation rate constants of $(1–5)\times10^{-4}\,M^{-1}\,s^{-1}$ that suggest a mild substituent effect on the CH acidity; this also is confirmed by the mild sensitivity of $E°$ of the $Ph_2CSAr^\bullet/Ph_2CSAr^-$ couple to the substituent. Addition of a proton donor mild enough to protonate Ph_2CH^- but not the radical anion formed in Equation (3), such as acetanilide ($pK_a^{DMF} = 22.3$),[25a] efficiently hampers the self-protonation reaction [Eq. (7)].

$$Ph_2CH^- + HA \rightarrow Ph_2CH_2 + A^- \quad (7)$$

Consequently, all electroactive compounds can now be reduced at the working potentials, and thus the current of the first peak increases to reach the expected two-electron stoichiometry. This is illustrated in Figure 1 for compound **1h** (solid line as opposed to the dashed curve). Whereas both the reduction and the oxidation peaks of Ph_2CSAr^- disappear, the oxidation peak of ArS^- remains (not shown in the figure), as thiophenols are the strongest acids in solution ($pK_a^{DMF} = 12.3$ and 6.8 for **1a** and **1h**, respectively).[25a,e]

Because the main goal of this part of the study was the determination of the heterogeneous ET parameters, all results described below and gathered in Table 2 were obtained in the presence of acetanilide (and thus under conditions in which the self-protonation reaction does not take place and the electrode reaction is a two-electron process). Besides the substituent effect on E_p, the results show that the peak widths ($\Delta E_{p/2}$, which is the absolute difference between E_p and the potential at mid-peak height) and consequently the corresponding values of the transfer coefficient α ($\Delta E_{p/2} = 1.857\,RT/F\alpha$)[27] do not significantly vary for **1a–d**; the peaks of **1h** and **1i**, however, yield larger α values. All α values are sufficiently large to ensure that the DET mechanism is stepwise.[1–3] For all compounds, when v increases $\Delta E_{p/2}$ also increases and thus α decreases. This is a general behavior indicating that reduction is controlled by a nonlinear dependence of the heterogeneous ET kinetics on E (i.e., the reaction thermodynamics). The reductions were thus studied by convolution analysis,[1a,21,28] which is an efficient tool for obtaining information on activation/driving force relationships and mechanistic transitions of DET reactions. By this approach the convoluted current I was calculated from background-subtracted voltammograms obtained at several scan rates (Figure 2). Convoluted current I is related to the real

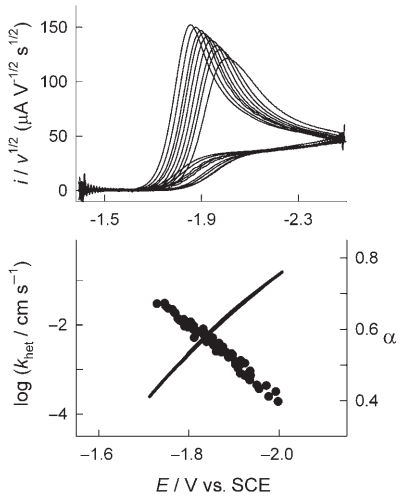

Figure 2. Cyclic voltammetry curves for the reduction of 2.0 mM **1h** in DMF/0.1 M TBAP at the GC electrode. The upper graph shows a series of background-subtracted curves at different scan rates (left to right: 0.1, 0.2, 0.5, 1, 2, 5, 10, 20, 50 V s^{-1}). The voltammetric current i is reported in its v-normalized form. The lower graph shows plots of the corresponding potential dependence of $\log k_{het}$ and α (full circles). $T = 25$ °C.

current i through the convolution integral[30] and thus displays a sigmoidal dependence on the applied potential E (see Figure S1 in the Supporting Information). For each experiment and sulfide, the I–E curves were characterized by the same limiting value I_l[29] within 2%. From the I_l values and by using electrodes of known area, the diffusion coefficients D of compounds **1** were calculated (Table 2).

The dependences on potential of the apparent (uncorrected for double-layer effects) heterogeneous rate constants k_{het} were obtained from the i, I, and D values,[29] as exemplified in Figure 2 for compound **1h**. The apparent values of α were obtained as a function of E by derivatization of the corresponding $\ln k_{het}$ versus E plots as $\alpha = -(RT/F)(\mathrm{d}\ln k_{het}/\mathrm{d}E)$. For all sulfides, the α versus E plots were linear within error, and thus point to an ET process controlled by a quadratic activation/driving force relationship and to the absence of ET-mechanism transitions.[4c] With these conditions attained, the $E°$ of the electrode reaction can usually be estimated as the E value at which $\alpha = 0.5$, as most models or calculations for outer-sphere or dissociative ET share the result that α should be about 0.5 at zero driving force.[9,10,12,14,30] The $E°$ values of sulfides **1** were thus estimated from the linear fit to the pertinent set of α versus E data. By using these $E°$ estimates, the apparent values of the standard rate constant $k°_{het}$ were obtained by parabolic fitting to the $\log k_{het}$ versus E plots. The consistency of the $E°$ and $k°_{het}$ values obtained by convolution analysis was also checked by digital simulation of the cyclic voltammograms, which led to very good reproduction of the experimental curves obtained by varying v by about 2.5 orders of magnitude. From the $k°_{het}$ values, using an Eyring-type equation ($\ln k°_{het} = \ln Z_{het} - \Delta G°^{\ddagger}_0/RT$) and the pertinent heterogeneous frequency factors Z_{het} ($Z_{het} = (RT/2\pi M)^{1/2}$, where M is the molar mass of the electroactive species), the heterogeneous intrinsic barriers $(\Delta G°^{\ddagger}_0)_{het}$ were calculated. The inner components $(\Delta G°^{\ddagger}_{0,i})_{het}$ were obtained by subtracting the $(\Delta G°^{\ddagger}_{0,s})_{het}$ component from $(\Delta G°^{\ddagger}_0)_{het}$; the $(\Delta G°^{\ddagger}_{0,s})_{het}$ values were calculated from the empirical equation $(\Delta G°^{\ddagger}_{0,s})_{het} = 13.9/r$,[21] where r [Å] is the sulfide radius obtained from the Stokes–Einstein equation and the experimental D value.

As shown in Table 2, the main outcome of this analysis is that the inner reorganization accompanying the reduction of **1a–d** accounts for about 60% of the intrinsic barrier (with no detectable substituent effect), whereas less inner reorganization affects the reduction of **1h** and **1i**. As already discussed,[15e] there are good reasons to believe that the $(\Delta G°^{\ddagger}_{0,i})_{het}$ behavior observed for **1a–d** is caused by a significant degree of spreading of the SOMO onto the cleaving C–S bond, and thus to an elongation of the latter on radical-anion formation. Finally, we employed the calculated intrinsic barriers and $E°$ values to simulate the CV behavior of **1h** and could estimate the C–S bond cleavage rate constant k_c to be 6×10^5 s^{-1}. For **1i**, k_c was also calculated from the CV analysis to be 11 s^{-1}.

The values discussed above were obtained by neglecting double-layer effects. In fact, the characterization of the double-layer properties of GC was carried out only very recently, by applying the Gouy–Chapman–Stern double-layer theory.[22] Application of such a correction, whose effect depends on the explored potential range and the potential region to which the experimental α or k_{het} data need to be extrapolated, does not change substantially the estimates of Table 2: typically, the $E°$ values become slightly more positive (the experimental error in the estimated $E°$ of "slow"

DET acceptors is already on the order of 0.1 V), the $\log k^{\circ}_{het}$ values increase by 0.4–0.6 units and the intrinsic barriers decrease by 0.6–0.8 kcal mol^{-1}, but the contribution of $(\Delta G^{\neq}_{0,i})_{het}$ to the latter decreases by no more than 5%. In the following, for consistency with previous work carried out on the reduction of other sulfides and disulfides at GC electrodes, double-layer effects will be neglected. In fact, our discussion will specifically focus on a comparison of the general trends displayed by the different series of compounds as a function of the substituents.

Indirect reduction of sulfides 1: The indirect reduction of **1** was accomplished by homogeneous redox catalysis with electrogenerated radical anions as homogeneous electron donors (D).[8] The mechanism of the ET reaction is analogous to that of the heterogeneous reduction, but the reduced form of the donor ($D^{\bullet -}$) replaces the electrode. The reaction sequence pertaining to sulfides **1** is shown in [Eqs. (8)–(11)], followed by carbanion protonation by the added acid, acetanilide [Eq. (7)].

$$D + e \rightleftharpoons D^{\bullet -} \quad (8)$$

$$D^{\bullet -} + Ph_2CHSAr \rightleftharpoons D + Ph_2CHSAr^{\bullet -} \quad (9)$$

$$Ph_2CHSAr^{\bullet -} \rightleftharpoons Ph_2CH^{\bullet} + ArS^{-} \quad (10)$$

$$D^{\bullet -} + Ph_2CH^{\bullet} \rightarrow D + Ph_2CH^{-} \quad (11)$$

In homogeneous redox catalysis experiments, the reversible CV peak of the mediator is transformed into a chemically irreversible, catalytic peak on addition of the acceptor. The current of the catalytic peak depends on the scan rate and the concentration of the acceptor: the ET rate constant k_{hom} [Eq. (9), forward reaction] is obtained by studying such dependences. Because of the presence of 1 equiv of acetanilide, required to hamper the self-protonation reaction, we avoided using mediators displaying some basicity, such as azobenzene derivatives. It is common protocol to choose mediators having E° values (E°_D) at least 200 mV more positive than the acceptor E_p at low scan rate, but in this study we also aimed at verifying whether it could have been possible to "push" the experimental system by using mediators with E° values similar to or even more negative than the acceptor E_p. Figure 3, which pertains to **1h** and to a mediator (anthracene) with an E° that is 70 mV more negative than the acceptor E_p at 0.2 V s^{-1}, nicely illustrates the outcome of such experiments. The catalytic (and complete) reduction of the acceptor occurs at potentials (prepeak to the mediator peak) that are more positive than either the donor or acceptor peak. We could verify that this is indeed a possible experimental strategy, as the experimental curves could be simulated very well; for the case shown in Figure 3, we could calculate a homogeneous ET rate constant as large as 5×10^{7} M^{-1} s^{-1}. With sulfides **1a** and **1c**, we could use mediators with E° values almost as negative (30–40 mV) as the acceptor E_p. A typical $\log k_{hom}$ versus E°_D plot (sulfide **1h**) is shown in Figure 4, while the other plots are provided in Figures S2–S5 in the Supporting Information, together with all ET rate constants (see Table S1).

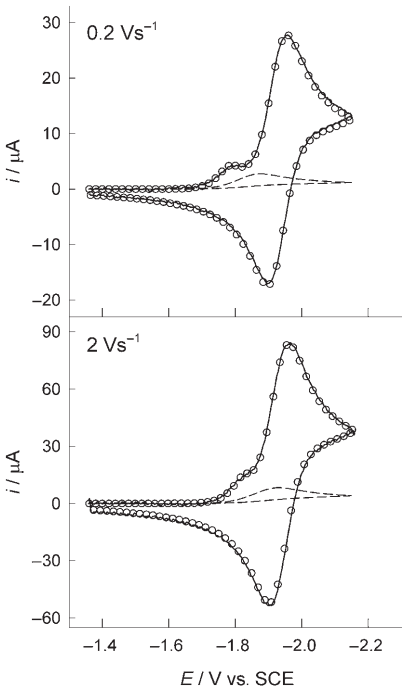

Figure 3. Cyclic voltammetry curves for the reduction of 0.1 mM **1h** in DMF/0.1 M TBAP at two scan rates. The CVs were obtained in the absence (dashed lines) and presence of 1.0 mM anthracene (solid lines). Simulations of the catalyzed reductions are shown by open circles. GC electrode, T = 25 °C.

According to the steady-state treatment of the kinetic Scheme illustrated above, the forward rate constant of reaction (9) k_{hom} can be expressed as in Equation (12).

$$\frac{1}{k_{hom}} = \frac{1}{k_d} + \frac{1}{Z_{hom}\exp(-\Delta G^{\neq}/RT)} + \frac{1}{k_d\exp(-\Delta G^{\circ}/RT)} \quad (12)$$

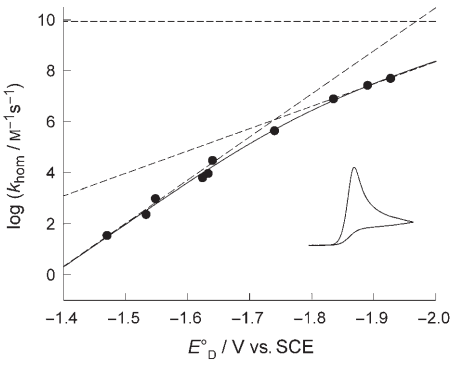

Figure 4. Plot of the logarithm of the homogeneous ET rate constant against E°_D for the reduction of **1h** by aromatic radical anions in DMF/0.1 M TBAP at 25 °C. The peak shows where the direct reduction of **1h** takes place at 0.2 V s^{-1}. The dashed lines illustrate the three regions, while the solid line is the fit to Equation (12).

Here k_d is the diffusion-controlled rate constant in DMF ($8.7\times10^9\,M^{-1}s^{-1}$)[15c] and Z_{hom} the collision frequency (average value $3\times10^{11}\,M^{-1}s^{-1}$), given by $Z=d^2[8\pi k_BT/\mu]^{1/2}$, where d is the encounter distance, k_B the Boltzman constant, and μ the reduced mass);[9a] the solution ET is considered adiabatic. $\Delta G^{\neq}$ can be expressed either as in the Marcus equation [Eq. (13), where one of the two reactants is neutral] or as a linear function of $\Delta G°$ (neglecting the variation of the ET coefficient with the driving force near $E°$).[31]

$$\Delta G^{\neq}=\Delta G_0^{\neq}\left(1+\frac{\Delta G^{\circ}}{4\Delta G_0^{\neq}}\right)^2 \qquad (13)$$

Because of the form of the right-hand side of Equation (12), $\log k_{hom}$ versus E_D° can be partitioned into three regions that are controlled by the diffusion of the reactants, the actual ET within the solvent cage, and product escape from the solvent cage (counterdiffusion); for the first and the last regions, the acceptor $E°$ can be estimated.[8,31]

Analysis of the data pertaining to ET to sulfides **1a–d,h** by a series of mediators led to the results gathered in Table 3. For **1a–d** plots with a slope corresponding to the activation-controlled region (Supporting Information) were obtained. The experimental data were linearly fitted to Equation (12) by using α_{hom} and $\log k_{hom}^{\circ}$ (the homogeneous ET coefficient and standard rate constant, respectively) as adjustable parameters[31] and the heterogeneous ET estimates of the $E°$ values. As shown in Table 3, the α_{hom} values were slightly larger than 0.5, while the corresponding α values obtained from CV measurements at low scan rate (Table 2) were generally smaller. This is in keeping with the fact that the homogeneous reductions are generally carried out at lower driving forces than the corresponding heterogeneous processes (the mediators have less negative $E°$ values than the applied potentials in direct electroreductions). From the $\log k_{hom}^{\circ}$ results, the corresponding intrinsic barriers could be obtained by using the above Z_{hom} value and the Eyring-type equation $\ln k_{hom}^{\circ}=\ln Z_{hom}-(\Delta G_0^{\neq})_{hom}/RT$.

Table 3. Electrochemical and kinetic parameters for the homogeneous reduction of sulfides **1** in DMF/0.1 M TBAP at 25 °C.

1	E_{hom}° [a] [V]	α_{hom} [b]	$\lg k_{hom}^{\circ}$ [b] [$M^{-1}s^{-1}$]	$(\Delta G_0^{\neq})_{hom}$ [b] [kcal mol^{-1}]	$(\Delta G_{0,i}^{\neq})_{hom}$ [b] [kcal mol^{-1}]
a	−2.40	0.55, 0.56	6.1, 5.7	7.3, 7.9	4.2, 4.8
b	−2.35	n.a., 0.53	5.9, 5.4	7.6, 8.3	4.4, 5.0
c	−2.27	0.53, 0.52	5.9, 5.5	7.6, 8.2	4.3, 4.9
d	−2.21	0.53, 0.53	6.2, 5.2	7.2, 8.3	4.3, 5.4
h	−1.97	0.77, 0.58	8.1, 8.1	4.7, 4.6	1.6, 1.5

[a] Determined from best fit of the redox catalysis data to Equation (12); for details and uncertainties, see text. [b] The first and second figures refer to the values obtained by using the convolution and redox-catalysis $E°$ values, respectively.

That the $\log k_{hom}$ versus E_D° plots of **1a–d** showed no indication of a counterdiffusion region can be related either to a small value of k_{hom}° or to a very fast cleavage reaction,[32] which would extend the activation-controlled region at the expense of the onset of the counterdiffusion-controlled zone. In both cases, we can take the most positive $\log k_{hom}$ value (most endergonic ET reaction) and impose a counterdiffusion line with appropriate slope [i.e., $-F/(RT\ln10)$]. If k_{hom}° is indeed small, minimum (i.e., more negative) values of $E°$ (of **1a–d**) can be estimated by extrapolation of the line to the diffusion-controlled region.[8,11b] If the counterdiffusion zone is positively shifted by the occurrence of fast cleavage in the solvent cage, the estimated $E°$ values provide maximum values (i.e., less negative), and the maximum positive deviation from the "true" $E°$ value is about 0.12 V.[8] Interestingly, (Table 3) these $E°$ estimates are indeed quite similar (but consistently more positive) to the heterogeneous ET estimates (Table 2): this is in agreement with either the occurrence of very fast C–S bond cleavages or small k_{hom}° values and the fact that the heterogeneous $E°$ data of Table 2 are not corrected for the double layer (which would cause a positive shift of the apparent $E°$ values). Indeed, the cleavage rates of compounds **1–3** (see below) would suggest that the second hypothesis is more likely.

For **1h**, we used the same procedure that was previously applied to study homogeneous ET to the similar sulfide **2h**.[15c] Thus, a Marcusian form of the $\Delta G°$ dependence of the activation-controlled process [Eqs. (12) and (13)] was employed. As shown in Figure 4, **1h** displays both activation and the counterdiffusion regions, and this allowed us to safely (k_c is sufficiently small, i.e., $6\times10^5\,s^{-1}$) calculate the homogeneous $E°$ from fitting of the $\log k_{hom}$ versus $E_{D/D^{\cdot-}}^{\circ}$ data. The $(\Delta G_0^{\neq})_{hom}$ value was also obtained as a fitting parameter; in another analysis of the data, however, we employed the heterogeneous $E°$ and recalculated $(\Delta G_0^{\neq})_{hom}$ (both values are shown in Table 3). As for the heterogeneous processes, the $(\Delta G_{0,i}^{\neq})_{hom}$ values were obtained by subtracting from the $(\Delta G_0^{\neq})_{hom}$ values the $(\Delta G_{0,s}^{\neq})_{hom}$ that were calculated from the empirical equation $(\Delta G_{0,s}^{\neq})_{hom}=24[(2r_D)^{-1}+(2r)^{-1}-(r_D+r)^{-1}]$,[33] in which we used $r_D=3.8$ Å as the average donor radius.

Concerning the C–S bond cleavage reaction, as already mentioned, the k_c values could be determined by CV analysis of the reduction peaks of **1h** and **1i**. By using the redox-catalysis approach, the k_c value for **1b** could be calculated. The method requires that the catalysis rate decreases as the concentration of D increases.[34] By using 9-phenylanthracene and varying its concentration in the range of 1–20 mM, results were obtained (the catalytic efficiency as a function of the pertinent kinetic parameter is shown in Figure S6 in the Supporting Information) that allowed the calculation of $k_c=9\times10^7\,s^{-1}$.

Direct reduction of sulfides 2: The CVs of sulfides **2a,b,d** are quite similar and show single irreversible peaks located at progressively more positive potentials. The peaks are more positive by 0.23–0.26 V than those of the corresponding sulfides **1**. Addition of weak acids to the solution does not affect these reduction peaks. The reduction of **2f** shows an irreversible peak followed by a reversible peak with $E°=$

−2.53 V. This is attributed to reduction of the corresponding thiolate formed in the DET reaction [Eqs. (14)–(16)]. In fact, and analogously to the behavior observed for the other sulfides, an oxidation peak (the E_p of which correlates well with the potentials of other *para*-substituted phenyl thiolates; by using the equation $E° = 0.069 + 0.619\sigma$, its $E°$ is estimated to be +0.38 V)[11b] attributable to thiolate oxidation was detected during the backward positive-going scan. Both the reduction and the oxidation peaks do not disappear on addition of weak acids, as the thiolate is the conjugate base of a relatively strong SH acid. However, the current of the first peak increases (by a factor of 0.5 at 0.2 V s^{-1}) when 1 equiv of acetanilide is added to the solution. The CV analysis indicates that a father–son reaction (such as self-protonation: whereas the pK_a^{DMF} of acetophenone is 25.3, that of the exogenous acid, acetanilide, is 22.3),[25a,c] affects the electroreduction mechanism, as already discussed for sulfides **1**.

The first irreversible peak of **2h** is followed by a small peak at low scan rates ($v < 1$ V s^{-1}) caused by the basic hydrolysis of the cyano group, as already discussed in detail;[15c,35] addition of a mild proton donor (*N*-cyclohexyl isobutyramide, $pK_a^{DMF} = 27.9$)[25a,26b] is sufficient to hamper this reaction. Addition of stronger acids does not affect the current of the reduction peak. The CV behavior of compound **2i** has been already described in detail.[20d] The first peak is irreversible, even at −30 °C and up to 1000 V s^{-1}, but its $E°$ could be estimated from redox-catalysis data to be −1.00 V. As for **2f**, the reversible reduction of the corresponding thiolate is observed at more negative potentials ($E° = -1.52$ V).

For compounds **2a**,**b**,**d**,**f**,**h**, if sufficiently anhydrous conditions are attained,[15a] the oxidation peak of Ph_3C^- can be observed; for **2i**, the peak related to the triphenylmethyl fragment is detected during the negative-going scan and is due to the reduction of $Ph_3C^{\cdot}$. At sufficiently high scan rates or in the presence of activated alumina, the peak of the redox couple $Ph_3C^{\cdot}/Ph_3C^-$ becomes reversible ($E° = -1.10$ V).[4a,20d] For **2b**,[4a] **2h**,[15c] and **2i**,[20d] the rate constants for C–S bond cleavage k_c were previously calculated from redox-catalysis data to be 8×10^{11}, 1.2×10^8, and 4.1×10^5 s^{-1}, respectively.

$$Ph_3CSAr + e \rightleftharpoons Ph_3CSAr^{\cdot -} \quad (14)$$

$$Ph_3CSAr^{\cdot -} \rightleftharpoons Ph_3C^{\cdot} + ArS^- \quad (15)$$

$$Ph_3C^{\cdot} + e \rightarrow Ph_3C^- \quad (16)$$

The heterogeneous ET kinetics of sulfides **2** were studied by convolution analysis at the GC electrode. The corresponding $E°$, $\log k_{het}^{\circ}$, $(\Delta G_0^{\neq})_{het}$, and $(\Delta G_{0,i}^{\neq})_{het}$ values were calculated as explained for sulfides **1**. The results (Table 4) show that the trend already discussed for sulfides **1** is even more pronounced. In particular, the inner reorganization accompanying the reduction of **2a**,**b**,**d** now accounts for as much as 65–70% of the intrinsic barrier (as opposed to about 60% for **2a**–**d**). For larger σ values, the role of $(\Delta G_{0,i}^{\neq})_{het}$ becomes less pronounced, but it is still noticeable. As already discussed for sulfides **1** and **2h**,[15c] the substituent-dependent sluggishness of the heterogeneous reduction of **2** is attributed to a more or less pronounced elongation of the C–S bond on radical-anion formation.

Table 4. Electrochemical and kinetic parameters for the heterogeneous reduction of **2** in DMF/0.1 M TBAP at 25 °C.

2	E_p[a] [V]	$\Delta E_{p/2}$[a] [mV]	α[b]	$E°$[c] [V]	$\lg k_{het}^{\circ}$[c] [cm s^{-1}]	$(\Delta G_0^{\neq})_{het}$ [kcal mol^{-1}]	$(\Delta G_{0,i}^{\neq})_{het}$ [kcal mol^{-1}]
a	−2.26	125	0.382	−1.97	−3.94	10.2	6.9
b	−2.21	113	0.423	−1.96	−3.84	10.1	6.7
d	−2.12	120	0.399	−1.89	−3.60	9.7	6.6
f	−1.61	82	0.582	−1.62	−2.08	7.6	4.5
h	−1.73	89	0.536	−1.72	−2.06	7.6	4.4
i	−0.88			−1.00			

[a] Measured at 0.2 V s^{-1}. [b] Measured from $\Delta E_{p/2}$. [c] The experimental uncertainty associated with the parameters obtained at $\alpha = 0.5$ is 40 mV ($E°$) and 0.3–0.4 lg units ($\lg k_{het}^{\circ}$).

Direct reduction of disulfides 3 and 4b: With the exception of **3i**, reduction of dibenzyl disulfides **3** occurs at much more negative potentials (0.6–0.7 V) than for the corresponding *para*-substituted diaryl disulfides **5**;[11b] this points to a very large effect brought about by the presence of a single methylene spacer between the aryl portion and the S–S bond. Figure 5 compares the CV curves (first peak) of the unsubstituted compounds **1b**, **2b**, **3b**, **4b**, and **5b**, together with the range spanned by each series from *p*-OMe to *p*-CN. The nitro derivatives were not included because these compounds must be considered to be substituted nitro compounds rather than nitro-substituted disulfides or sulfides. Figure 5 also displays the reduction peak of disulfide **4b**, which shows that addition of a further methylene spacer to **3b** does not modify the pattern significantly; the difference in E_p is only 0.06 V.

The voltammetric patterns of disulfides **3** are generally more complex than those of compounds **1**, **2**, and **5**. The CVs of **3a, 3b**, and **3d**, however, are quite similar and thus can be discussed together. A typical CV shows a single irreversible reduction peak and, on the positive-going scan, the

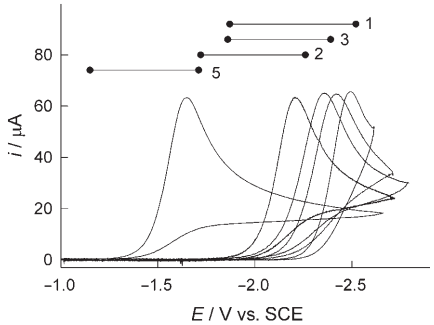

Figure 5. Comparison between the CV curves (0.2 V s^{-1}) of (left to right) **5b**, **2b**, **3b**, **4b**, and **1b** in DMF/0.1 M TBAP at 25 °C. The horizontal lines show the range spanned for series **5**, **2**, **3**, and **1** from the *para*-methoxy to the *para*-cyano derivatives.

oxidation peak associated with thiolate oxidation. On addition of acetic acid (weaker acids such as phenol and trifluoroethanol do not affect the CV behavior), the reduction peak does not change its shape and current, but a second peak develops at more negative potentials (0.39–0.64 V, depending on the substituent). Increasing the amount of acid in the disulfide solution does not affect the first peak, but the peak current of the second peak progressively increases. This second peak is coincident with the peak that can be observed by reducing the corresponding thiol in the presence of the same acid (independent experiments carried out with the thiols). When the amount of acid in the thiol solution increases, the peak current also increases, as already mentioned for the disulfides: this outcome indicates that thiol reduction entails hydrogen evolution and thiolate formation, followed by regeneration of the thiol through protonation. In the case of the thiol of **3d**, however, reduction occurs in two steps. The first peak, which is weakly acid dependent, appears to correspond to reductive cleavage of the C–Cl bond (at 0.2 V s^{-1}, $E_p = -2.55$ V) to form $PhCH_2SH$; in fact, the current of the second peak is dependent on the amount of acid and the peak has the same E_p as $PhCH_2SH$, that is, the thiol of **3b**.

Therefore, the reduction of **3a**, **3b**, and **3d** occurs by S–S bond cleavage to form the thiolate and the thiyl radical; at the working potentials, the latter is rapidly reduced to form another thiolate ion. The peaks of **3a, 3b**, and **3d** obtained in the absence of acid (but similar results were obtained in the presence of phenol) were analyzed by convolution analysis, which led to the $E°$ and k°_{het} data shown in Table 5. The same analysis was applied to **4b**, which undergoes reduction along similar lines as its shorter homologue **3b**. It is noteworthy that the k°_{het} values of these disulfides are very small, much smaller than those of the corresponding sulfides. The values are very similar to those previously obtained for a series of dialkyl disulfides.[12] Because of the present findings, and in line with the conclusions of the last-named investigation, the electroreduction of **3a, 3b**, and **3d** is ascribed to a dissociative S–S bond cleavage proceeding through formation of a loose radical anion, the SOMO of which is essentially coincident with the S–S σ* antibonding orbital.

The electroreduction of the thiol corresponding to disulfide **3i** already shows some chemical reversibility at 0.2 V s^{-1}; its $E°$ value of −1.11 V is more positive than that of *para*-nitrotoluene (−1.16 V). On acid addition, the peak current progressively increases, which indicates that the reduction entails thiolate formation (and thus hydrogen evolution) followed by thiol regeneration by protonation. The thiolate, obtained on addition of a base to the thiol solution, is also reducible and its peak displays some reversibility at low scan rates ($E° = -1.30$ V). With this information, the reduction behavior of **3i** can be easily accounted for. The reduction of **3i** (at 0.2 V s^{-1}, $E_p = -1.09$ V) occurs at the same potential as that of the thiol; at low scan rates, the peak is chemically irreversible and a second reduction peak, with same E_p as the thiolate, is observed. On acid addition, essentially the same CV pattern as for the thiol is observed: the current, however, is twice as large as that of the thiol. By overlapping the CVs of **3i**, thiol, and *para*-nitrotoluene, it is evident that the latter does not form and thus that the reduction of **3i** does not involve C–S bond cleavage (see below). To conclude, the reduction of **3i** involves radical-anion formation, and the SOMO is located at the nitro group; intramolecular DET and then S–S bond cleavage follow. The peak of **3i** starts displaying reversibility as the scan rate increases (at ca. 1 V s^{-1}), while the peak attributed to the thiolate disappears. The reversible peak, however, is broad. This is because reduction may occur on both nitro groups and this makes injection of a second electron into the second nitro group slightly less favorable.[27c] Digital simulation of the CV curves obtained at different scan rates allowed $E°$ values of −1.05 and −1.11 V to be estimated, and the difference in $E°$ was indeed on the order of the expected value (36 mV).[27c] The k°_{het} of the initial ET is essentially the same as that of the nitro derivatives described above.

The CV patterns of the cyano derivatives **3g** and **3h** (first reduction peak at −1.98 and −1.85 V, respectively) are complicated by the presence of several peaks that are dependent on the presence or absence of a weak acid. We describe here the results obtained for **3h** (cf. Figure S7 in the Supporting Information); the main features of the CV behavior of **3g** are similar. A first indication of more complexity comes from the fact that the peak for *para*-cyanotoluene is present in the CV pattern. This implies that C–S bond cleavage occurs rather than S–S bond cleavage. A possible mechanism is thus initial formation of a π* radical anion (the thiol of **3h** is reducible at slightly more negative potentials) followed by intramolecular DET. Cleavage of a C–S bond forms the corresponding hydrodisulfide anion and the *para*-cyanobenzyl radical, which is rapidly reduced to the carbanion (its reduction potential in CH_3CN is −0.77 V).[36] Depending on the availability of protons in solution or by addition of a weak acid, such as acetanilide, the carbanion is protonated to form *para*-cyanotoluene ($E° = 2.39$ V). Other peaks related to the hydrodisulfide anion (−2.25 V at 0.2 V s^{-1}) and products derived from its irreversible reduction are also present. Interestingly, the thiol of **3h** undergoes a similar reduction mechanism that yields

Table 5. Electrochemical and kinetic parameters for the heterogeneous reduction of **3** and **4b** in DMF/0.1 M TBAP at 25 °C.

Disulfide	E_p[a] [V]	$\Delta E_{p/2}$[a] [mV]	α[b]	E°_{het} [V]	$\lg k^\circ_{het}$ [cm s^{-1}]	$(\Delta G^{\neq}_0)_{het}$ [kcal mol^{-1}]	$(\Delta G^{\neq}_{0,i})_{het}$ [kcal mol^{-1}]
3a	−2.39	127	0.376	−1.88	−5.70	12.6	9.5
3b	−2.36	129	0.370	−1.84	−5.53	12.5	8.7
4b	−2.42	132	0.361	−1.91	−5.58	12.5	9.2
3d	−2.15	124	0.385	−1.75	−4.90	11.5	7.9
3i	−1.09	55	0.852	−1.05	−1.10	6.3	3.1

[a] Measured at 0.2 V s^{-1}. [b] Measured from $\Delta E_{p/2}$.

para-cyanotoluene by C–S bond cleavage. Because of the complexity of the reductions of **3g** and **3h** and particularly the fact that the mechanism is different from that of the other disulfides of series **3** (and **4b**) and **5**, we prefer not to include the data of these compounds in the following discussion.

DET mechanisms and intrinsic barriers: The heterogeneous and homogeneous kinetic data of sulfides and disulfides point to a common reduction mechanism for the acceptors with electron-donating or mildly electron-withdrawing ring substituents. As the Hammett σ value becomes larger than 0.1–0.2, the intrinsic barriers decrease until, with the nitro derivative, the typical values of nondissociative-type nitro compounds is attained. Figure 6 illustrates the progressive

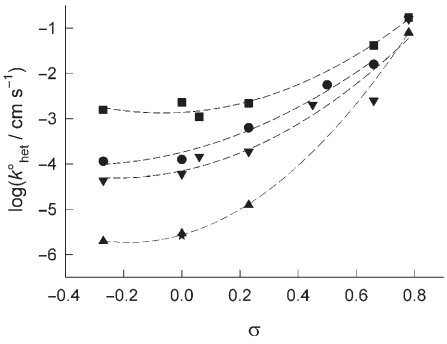

Figure 6. Hammett plot of the logarithm of the heterogeneous ET rate constant for the reduction of sulfides **1** (■), sulfides **2** (●), disulfides **5** (▼), disulfides **3** (▲), and **4b** (∗) in DMF/0.1 M TBAP at 25 °C. The dashed lines are only intended to emphasize the experimental trends.

variation of $\log k^{\circ}_{het}$ of compounds **1**, **2**, **3**, and **5**[11] as a function of σ. Subtraction of the solvent-reorganization energies from the $(\Delta G_0^{\neq})_{het}$ and $(\Delta G_0^{\neq})_{hom}$ values shows that the decrease in the standard rate constants at low σ values is caused by a progressive increase in $\Delta G^{\neq}_{0,i}$. The larger the value of $\Delta G^{\neq}_{0,i}$ the larger the extent of localization of the SOMO onto the region of the cleaving bond.

As illustrated in Figure 6, the decrease is more marked as one goes from compounds **1**, to **2**, to **5**, to **3**. For sulfides **1**, inner reorganization is relatively small, even at low σ values. On the other hand, sulfides **2** and diaryl disulfides **5** show similar values and larger $\Delta G^{\neq}_{0,i}$ values. Whereas for disulfides **5** we already showed both experimentally and through calculations that $\Delta G^{\neq}_{0,i}$ is related to elongation of the S–S bond on radical-anion formation, we have no specific information on the causes making $\Delta G^{\neq}_{0,i}$ of sulfides **2** almost as large as that of disulfides **5**. However, because calculations previously carried out for **2h** provide evidence of some elongation of the C–S bond on radical-anion formation,[15c] we expect that also for **2** elongation of the cleaving bond is the most important ingredient making $\Delta G^{\neq}_{0,i}$ large. The very large values of $\Delta G^{\neq}_{0,i}$ and thus very small values of $\log k^{\circ}$ of disulfides **3**, in which a methylene spacer separates the cleaving bond from the aryl moieties, point to a SOMO localized on the S–S bond, as typically found for dialkyl disulfides. Similar considerations apply to **4b**, which shows that, addition of a further methylene unit does not modify the picture significantly.

Relation between heterogeneous and homogeneous reductions: The heterogeneous kinetic data can be compared to the corresponding homogeneous kinetic data through the pertinent intrinsic barriers $(\Delta G_0^{\neq})_{het}$ and $(\Delta G_0^{\neq})_{hom}$. Whereas the former needs no corrections, the $(\Delta G_0^{\neq})_{hom}$ values refer to the standard rate constant k°_{hom} and thus to the ET rate constant from a hypothetical donor with the same E°. $(\Delta G_0^{\neq})_{hom}$ can be transformed into the homogeneous self-exchange value $(\Delta G_0^{\neq})_{hom,ex}$ by using the cross-relation shown in Equation (17).

$$(\Delta G_0^{\neq})_{hom} = [(\Delta G_0^{\neq})_{hom,ex} + (\Delta G_0^{\neq})_{hom,ex,D/D^{\cdot -}}]/2 \qquad (17)$$

For the homogeneous self-exchange value of the donor $(\Delta G_0^{\neq})_{hom,ex,D/D^{\cdot -}}$, which can be considered to be approximately constant for the donors commonly employed, we used 3.6 kcal mol^{-1}.[37] For consistency, we used the $(\Delta G_0^{\neq})_{hom}$ values corresponding to the E° determined by convolution analysis. The resulting $(\Delta G_0^{\neq})_{het}$ and $(\Delta G_0^{\neq})_{hom,ex}$ data of compounds **1**, **2** and **5** are plotted in Figure 7; the $(\Delta G_0^{\neq})_{hom,ex}$

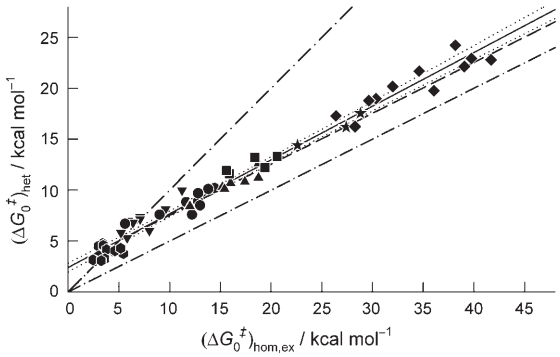

Figure 7. Correlation between heterogeneous and homogeneous intrinsic barriers for different classes of ET acceptors: aromatic compounds (⬢), benzyl aryl ethers and haloaromatic compounds (▼), sulfides (●), disulfides (▲), peroxides (■), haloacetonitriles (★), and alkyl halides (◆). The solid line is the best linear fit to the data, while the dotted lines show the 99% confidence intervals. The two dash-dotted lines illustrate the Hush (upper line) and Marcus (lower line) behaviors. The dashed curve represents the Hush prediction with a steady increase in inner reorganization (see text).

values of sulfides **2** and disulfides **5** were obtained from refs. [4a], [11b], [15c], and [16]. Figure 7 also displays a number of additional ET data, also obtained in DMF and treated as above. In particular, we added $\Delta G_0^{\neq}$ values pertaining to: 1) outer-sphere aromatic acceptors forming stable radical anions;[37] 2) stepwise-DET acceptors such as benzyl aryl ethers,[1a] halobenzenes, and halopyridines;[38] 3) other cases of stepwise DET involving formation of loose radical anions and cleavage of the C–S[15a] or S–S bond;[39]

4) concerted-DET acceptors involving ion–dipole interactions, such as haloacetonitriles;[14,40] 5) adiabatic concerted DET acceptors such as alkyl halides,[19,41] benzyl bromide,[13,42] benzyl chloride,[41b,43] and perfluoroalkyl halides;[44] 6) nonadiabatic concerted DET acceptors such as dialkyl peroxides,[21,33] endoperoxides,[45] and peresters.[4d,46]

Figure 7 shows the important result that, independent of the actual ET or DET mechanism and despite the different sources, the $(\Delta G_0^{\neq})_{het}/(\Delta G_0^{\neq})_{hom,ex}$ data correlate very well.[47] The figure also shows the trends expected according to the Marcus[48] and Hush[18] models for outer-sphere ET. From the point of view of the intrinsic barriers, the two models differ in the magnitude of the solvent-reorganization energy for heterogeneous ET: whereas in the Hush treatment the acceptor (located at the reaction site) is viewed as sufficiently distant from the electrode surface that the effect of the image charge can be neglected, this effect is included in the Marcus model. We also note that these models are independent of whether the acceptor undergoes reductive cleavage of a σ bond, and thus similar arguments can be applied to DET. The heterogeneous and homogeneous solvent-reorganization barriers are thus related by the following Marcus [Eq. (18), where the acceptor–electrode distance is half the donor–acceptor separation in the homogeneous case] and Hush [Eq. (19)] expressions.

$$(\Delta G_{0,s}^{\neq})_{het} = 0.5\,(\Delta G_{0,s}^{\neq})_{hom,ex} \tag{18}$$

$$(\Delta G_{0,s}^{\neq})_{het} = (\Delta G_{0,s}^{\neq})_{hom,ex} \tag{19}$$

Both models describe the inner component in the same way, that is, the homogeneous value is twice the heterogeneous value, as in the latter case only one molecule reorganizes [Eq. (20)].

$$(\Delta G_{0,i}^{\neq})_{het} = 0.5\,(\Delta G_{0,i}^{\neq})_{hom,ex} \tag{20}$$

By using Equations (18)–(20) it follows that the relationship between the heterogeneous and homogeneous intrinsic barriers is different: in the Marcus case Equation (21) applies, but Equation (22) holds in the Hush treatment.

$$(\Delta G_0^{\neq})_{het} = 0.5\,(\Delta G_0^{\neq})_{hom,ex} \tag{21}$$

$$\begin{aligned}(\Delta G_0^{\neq})_{het} &= 0.5\,(\Delta G_{0,i}^{\neq})_{hom,ex} + (\Delta G_{0,s}^{\neq})_{hom,ex} \\ &= 0.5\,(\Delta G_0^{\neq})_{hom,ex} + 0.5\,(\Delta G_{0,s}^{\neq})_{hom,ex}\end{aligned} \tag{22}$$

In the Marcus case, $(\Delta G_0^{\neq})_{het}$ is a linear function of $(\Delta G_0^{\neq})_{hom,ex}$ (Figure 7, lower dash-dotted line, slope 0.5). The same is true in Equation (21) for low barriers (simple outer-sphere ET) in which solvent reorganization is the only term contributing to the barrier. Under these conditions the Hush slope is unity (Figure 7, upper dash-dotted line). If we consider that the radii of common acceptors and donors are about 3.8 Å, a reasonable limiting value of $(\Delta G_{0,s}^{\neq})_{hom,ex}$ is 5.1 kcal mol^{-1}, as obtained from Equation (23)[18,48] (van der Waals contact in the solvent cage).

$$(\Delta G_{0,s}^{\neq})_{hom,ex} = \frac{N_A e^2}{16\pi\varepsilon_0}\left(\frac{1}{\varepsilon_{op}} - \frac{1}{\varepsilon_S}\right)\left(\frac{1}{2r_D} + \frac{1}{2r} - \frac{1}{r_D + r}\right) \tag{23}$$

Here e is the charge of the electron, ε_0 is the permittivity of vacuum, and ε_{op} and ε_s are the optical and static dielectric constants of the solvent. By using this $(\Delta G_{0,s}^{\neq})_{hom,ex}$ value and increasing the inner component, the Hush relationship [Eq. (22)] takes the form shown in Figure 7 (dashed line). Therefore, for sufficiently large $\Delta G_0^{\neq}$ values ($(\Delta G_0^{\neq})_{hom,ex} >$ 6–7 kcal mol^{-1}) the two equations describe lines with the same slope. In the Hush formulation, however, the intercept has a nonzero value of 2.5 kcal mol^{-1} ($(\Delta G_{0,s}^{\neq})_{hom,ex}/2$).

This is exactly, within error, what we observe in the experimental plot of Figure 7. Linear fit of the data (solid line) yields Equation (24).

$$(\Delta G_0^{\neq})_{het} = 2.391 + 0.528\,(\Delta G_0^{\neq})_{hom,ex} \tag{24}$$

The quality of the correlation, which is based on a collection of 68 data points ($r^2 = 0.980$) encompassing a $(\Delta G_0^{\neq})_{hom,ex}$ range of 2–42 kcal mol^{-1}, is worth stressing because it now is possible to predict (99% confidence) the values of $(\Delta G_0^{\neq})_{het}$ and $(\Delta G_0^{\neq})_{hom,ex}$ to within 0.5–1 and 1–2 kcal mol^{-1}, respectively. According to our extrapolation the average $(\Delta G_{0,s}^{\neq})_{hom,ex}$ is thus 4.8 kcal mol^{-1}, which is slightly smaller than the value calculated from Equation (23) but larger than that obtained with the above-mentioned empirical approach.

The ETs of Figure 7 can be roughly classified into four groups. First, there is outer-sphere ETs forming either stable radical anions or, for stepwise DETs, "stiff" radical anions. For these acceptors $\Delta G_{0,s}^{\neq}$ is the most important contribution to $\Delta G_0^{\neq}$. Because for common molecules (r = 3–4 Å) the $(\Delta G_{0,s}^{\neq})_{hom,ex}$ value is in the range of 3–5 kcal mol^{-1} ($(\Delta G_{0,s}^{\neq})_{het}$ are similar), typical values of $(\Delta G_0^{\neq})_{hom,ex}$ [transposition to the corresponding heterogeneous values can be made through Eq. (24)] for simple outer-sphere acceptors can be taken as those within about 5 kcal mol^{-1}. The values slightly increase for stepwise DET forming rigid radical anions (benzyl aryl ethers and haloaromatic compounds) and, in fact, some aryl halides undergo non-negligible inner reorganization. When the SOMO partially involves the cleaving bond, as for several sulfides and, particularly, disulfides, bond elongation results in a large inner contribution, and $(\Delta G_0^{\neq})_{hom,ex}$ values can be as large as 17–19 kcal mol^{-1}. For concerted DETs, we collected values ranging from 16 to 42 kcal mol^{-1}. In fact, the intrinsic barrier of concerted DET is $\Delta G_0^{\neq} = BDE/4 + \Delta G_{0,s}^{\neq} + \Delta G_{0,i}^{\neq\prime}$, where the latter term does not include the contribution of the mode corresponding to the breaking A–B bond.[10] The BDE is the bond dissociation energy and is the dominant term. It may vary substantially: while peroxides have typical BDE values of 30–40 kcal mol^{-1}, alkyl halides have BDEs of 50–70 kcal mol^{-1}. Because of this, while the experimental $(\Delta G_0^{\neq})_{hom,ex}$ values of peroxides are 16–21 kcal mol^{-1}, those of halides are 26–42 kcal mol^{-1}. Ion–dipole interactions in the cage, however, may lower the barrier significantly: for example, halo acetonitriles have values of 23–29 kcal mol^{-1}.

To conclude, thanks to reliable and well-tested electrochemical protocols (for convolution analysis and homogeneous redox catalysis) and the variety of ET data accumulated since the 1980s (particularly by Savéant's group, the Aarhus school, and us), it now is possible to observe that the law governing the difference between the heterogeneous and homogeneous data is common to different types of ET, ranging from simple outer-sphere ETs to concerted DETs. These processes are ruled by a quadratic activation/driving force relationship of the Marcus or Savéant form. The correlation of Figure 7 also shows progressive variation of the intrinsic barriers: the barriers of the two borderline DET cases are similar, and those of peroxides (concerted DET) are even smaller than those of disulfides forming σ* radical anions. A significance of Equation (24) validating the Hush model is its predictability, because in many cases one of the intrinsic barriers is often difficult or impractical to obtain.

Acknowledgements

This work was financially supported by the Ministero dell'Istruzione, dell'Università e della Ricerca (MIUR, Italy), the Integrated Action Italy-Spain between the University of Padova and the Universidad de La Laguna, and the Natural Science and Engineering Research Council (NSERC) of Canada. A.B.M. is thankful to the Universidad de La Laguna y Caja Canarias for a PhD grant.

[1] a) F. Maran, D. D. M. Wayner, M. S. Workentin, *Adv. Phys. Org. Chem.* **2001**, *36*, 85–166; b) F. Maran, M. S. Workentin, *Interface* **2002**, *31*, 44–49.
[2] S. Antonello, F. Maran, *Chem. Soc. Rev.* **2005**, *34*, 418–428.
[3] J.-M. Savéant, *Adv. Phys. Org. Chem.* **2000**, *35*, 117–192.
[4] a) M. G. Severin, G. Farnia, E. Vianello, M. C. Arévalo, *J. Electroanal. Chem.* **1988**, *251*, 369–382; b) S. Antonello, F. Maran, *J. Am. Chem. Soc.* **1997**, *119*, 12595–12600; c) S. Antonello, F. Maran, *J. Am. Chem. Soc.* **1999**, *121*, 9668–9676; d) S. Antonello, F. Formaggio, A. Moretto, C. Toniolo, F. Maran, *J. Am. Chem. Soc.* **2001**, *123*, 9577–9584; e) F. Najjar, C. André-Barrès, M. Baltas, C. Lacaze-Dufaure, D. C. Magri, M. S. Workentin, T. Tzédakis, *Chem. Eur. J.* **2007**, *13*, 1174–1179.
[5] a) C. P. Andrieux, M. Robert, F. D. Saeva, J.-M. Savéant, *J. Am. Chem. Soc.* **1994**, *116*, 7864–7871; b) C. P. Andrieux, J.-M. Savéant, C. Tardy, *J. Am. Chem. Soc.* **1997**, *119*, 11546–11547; c) L. Pause, M. Robert, J.-M. Savéant, *J. Am. Chem. Soc.* **1999**, *121*, 7158–7159; d) C. Costentin, P. Hapiot, M. Médebielle, J.-M. Savéant, *J. Am. Chem. Soc.* **1999**, *121*, 4451–4460; e) C. Costentin, M. Robert, J.-M. Savéant, *J. Am. Chem. Soc.* **2004**, *126*, 16834–16840.
[6] A. Houmam, E. M. Hamed, I. W. Still, *J. Am. Chem. Soc.* **2003**, *125*, 7258–7265.
[7] M. A. Prasad, M. V. Sangaranarayanan, *Chem. Phys. Lett.* **2005**, *414*, 55–60.
[8] C. P. Andrieux, J.-M. Savéant, *J. Electroanal. Chem.* **1986**, *205*, 43–58.
[9] a) R. A. Marcus, *Ann. Pharm. Belg. Ann. Rev. Phys. Chem.* **1964**, *15*, 155–196; b) R. A. Marcus, N. Sutin, *Biochim. Biophys. Acta* **1985**, *811*, 265–322.
[10] J.-M. Savéant, *J. Am. Chem. Soc.* **1987**, *109*, 6788–6795.
[11] a) K. Daasbjerg, H. Jensen, R. Benassi, F. Taddei, S. Antonello, A. Gennaro, F. Maran, *J. Am. Chem. Soc.* **1999**, *121*, 1750–1751; b) S. Antonello, K. Daasbjerg, H. Jensen, F. Taddei, F. Maran, *J. Am. Chem. Soc.* **2003**, *125*, 14905–14916.
[12] S. Antonello, R. Benassi, G. Gavioli, F. Taddei, F. Maran, *J. Am. Chem. Soc.* **2002**, *124*, 7529–7538.
[13] A. Cardinale, A. Gennaro, A. A. Isse, F. Maran in *New Directions in Organic Electrochemistry, Vol. 2000-15*(Eds.: A. J. Fry, Y. Matsumura), The Electrochemical Society, New Jersey, **2000**, pp. 136–140.
[14] A. Cardinale, A. A. Isse, A. Gennaro, M. Robert, J.-M. Savéant, *J. Am. Chem. Soc.* **2002**, *124*, 13533–13539.
[15] a) M. G. Severin, M. C. Arévalo, G. Farnia, E. Vianello, *J. Phys. Chem.* **1987**, *91*, 466–472; b) M. C. Arévalo, G. Farnia, M. G. Severin, E. Vianello, *J. Electroanal. Chem.* **1987**, *220*, 201–221; c) M. G. Severin, M. C. Arévalo, F. Maran, E. Vianello, *J. Phys. Chem.* **1993**, *97*, 150–157; d) A. B. Meneses, S. Antonello, M. C. Arévalo, F. Maran, *Electrochim. Acta* **2005**, *50*, 1207–1215.
[16] S. Jakobsen, H. Jensen, S. U. Pedersen, K. Daasbjerg, *J. Phys. Chem. A* **1999**, *103*, 4141–4143.
[17] a) *The Chemistry of Sulphur-Containing Functional Groups, Suppl. S*, (Eds.: S. Patai, Z. Rappoport), Wiley, New York, **1993**; b) *S-centered Radicals* (Ed.: Z. B. Alfassi), Wiley, Chichester, **1999**; c) R. A. Rossi, A. B. Pierini, A. B. Peñéñory, *Chem. Rev.* **2003**, *103*, 71–167.
[18] N. S. Hush, *Electrochim. Acta* **1968**, *13*, 1005–1023.
[19] S. Antonello, F. Maran, *J. Am. Chem. Soc.* **1998**, *120*, 5713–5722.
[20] a) C. Finzi, V. Bellavista, *Gazzetta Chimica Italiana* **1932**, *62*, 699–709; b) G. Farnia, A. Ceccon, P. Ceselli, *J. Chem. Soc. Perkin Trans. 2* **1972**, 1016–1021; c) G. Farnia, M. G. Severin, E. Vianello, *J. Chem. Soc. Perkin Trans. 2* **1978**, 1–8; d) G. Capobianco, G. Farnia, M. G. Severin, E. Vianello, *J. Electroanal. Chem.* **1984**, *165*, 251–263; e) S. Tognato, Laurea thesis, University of Padova, Italy, **1991**.
[21] S. Antonello, M. Musumeci, D. D. M. Wayner, F. Maran, *J. Am. Chem. Soc.* **1997**, *119*, 9541–9549.
[22] A. B. Meneses, S. Antonello, M. C. Arévalo, F. Maran, *Electroanalysis* **2006**, *17*, 363–370.
[23] F. Maran, M. S. Workentin, unpublished results.
[24] a) R. Fuhlendorff, D. Occhialini, S. U. Pedersen, H. Lund, *Acta Chem. Scand.* **1989**, *43*, 803–806; b) D. D. M. Wayner, D. J. McPhee, D. Griller, *J. Am. Chem. Soc.* **1988**, *110*, 132–137; c) J. Gamby, P. Hapiot, J.-M. Savéant, *J. Am. Chem. Soc.* **2002**, *124*, 8798–8799.
[25] When not available, the pK_a^{DMF} values can be obtained from the corresponding data in DMSO[25b–e] by using the correlation $pK_a^{DMF} = 1.56 + 0.96\,pK_a^{DMSO}$.[25a] a) F. Maran, D. Celadon, M. G. Severin, E. Vianello, *J. Am. Chem. Soc.* **1991**, *113*, 9320–9329; b) F. G. Bordwell, W. S. Matthews, N. R. Vanier, *J. Am. Chem. Soc.* **1975**, *97*, 442–443; c) F. G. Bordwell, J. E. Bares, J. E. Bartmess, G. E. Drucker, J. Gerhold, G. J. McCollum, M. Van Der Puy, N. R. Vanier, W. S. Matthews, *J. Org. Chem.* **1977**, *42*, 326–332; d) W. N. Olmstead, Z. Margolin, F. G. Bordwell, *J. Org. Chem.* **1980**, *45*, 3295–3299; e) F. G. Bordwell, D. L. Hughes, *J. Org. Chem.* **1982**, *47*, 3224–3232.
[26] a) F. Maran, S. Roffia, M. G. Severin, E. Vianello, *Electrochim. Acta* **1990**, *35*, 81–88; b) F. Maran, *J. Am. Chem. Soc.* **1993**, *115*, 6557–6563.
[27] a) R. S. Nicholson, I. Shain, *Anal. Chem.* **1964**, *36*, 706–723; b) L. Nadjo, J.-M. Savéant, *J. Electroanal. Chem.* **1973**, *48*, 113–145; c) A. J. Bard, L. R. Faulkner, *Electrochemical Methods, Fundamentals and Application*s, 2nd ed., Wiley, New York, **2001**.
[28] J.-M. Savéant, D. Tessier, *J. Electroanal. Chem.* **1975**, *65*, 57–66.
[29] The convolution integral (J. C. Imbeaux, J.-M. Savéant, *J. Electroanal. Chem.* **1973**, *44*, 169–187) is: $I = \pi^{1/2} \int_{\geq} \frac{i(u)}{(t-u)^{1/2}} \delta u$
The *I–E* plot has a sigmoidal shape, and the limiting value is $I_l = nFAD^{1/2}C^*$, where n is the overall electron consumption, A the electrode area, D the diffusion coefficient, and C^* the substrate concentration. For a slow heterogeneous ET or when the latter becomes irreversible because of a fast follow-up reaction, such as bond cleavage, the potential-dependent heterogeneous rate constant $k_{het} = k_{het}(E)$ is obtained as a function of E through equation $\ln k_{het}(E) = \ln D^{1/2} - \ln[(I_l - I)/i]$.
[30] J.-M. Savéant, *J. Phys. Chem.* **1994**, *98*, 3716–3724.
[31] By assuming a linear activation/driving force relationship for the ET reaction, Equation (12) takes the following form:[8]
$\frac{1}{k_{hom}} = \frac{1}{k_d} + \frac{1}{k^\circ_{hom} \exp(-\alpha_{hom} \Delta G^\circ/RT)} + \left(\frac{1}{k_d} + \frac{1}{Z_{hom}}\right) \frac{1}{\exp(-\Delta G^\circ/RT)}$
where k°_{hom} is the homogeneous standard rate constant (corresponding to the value of the ET rate constant by a generic donor matching

the condition $\Delta G^\circ = 0$), and α_{hom} is the average homogeneous transfer coefficient.

[32] When the cleavage occurs within the timescale of the solvent cage (ca. 10^{-10} s), the third term of Equation (12) (counterdiffusion region) is more complex.[8] Therefore, for fast-cleaving radical anions ($k_c > 10^{10}\ s^{-1}$) the use of Equation (12) introduces further uncertainty in the determination of the acceptor E°; in particular, a lower limit of E° can only be assessed. Among the investigated sulfides, only for **1h** (radical-anion lifetime ≈ 1 μs) were rate-constant data clearly obtained in the counterdiffusion region.

[33] R. L. Donkers, F. Maran, D. D. M. Wayner, M. S. Workentin, *J. Am. Chem. Soc.* **1999**, *121*, 7239–7248.

[34] The method relies on the following reasoning. If the cleavage reaction can be considered as irreversible, the disappearance of $D^{\bullet-}$ (which is involved in reactions (9) and (11) is ruled by the following rate law, where k_{hom} and k_{-hom} refer to reaction (9): $-\frac{d[D^{\bullet-}]}{dt} = \frac{2k_c k_{hom}[Ph_2CHSAr]}{k_c + k_{-hom}[D]}[D^{\bullet-}]$
If $k_c \gg k_{-hom}[D]$, the rate-determining step is the forward ET step (9), but if the two terms in the denominator are comparable an increase of the concentration of D inhibits the reaction. If $k_c \ll k_{-hom}[D]$, the ET step is a pre-equilibrium reaction. In practice, when the $k_{-hom}[D]$ term is not negligible the catalytic increase R (ratio between the i_p values of the donor peak in the presence and in the absence of sulfide in solution) decreases as [D] increases: for any given combination of [D]/v the value of R, which is plotted against the kinetic parameter $\log RT[D]/Fv$, decreases when [D] is made sufficiently large. Typical plots are shown in the Supporting Information.

[35] M. C. Arévalo, F. Maran, M. G. Severin, E. Vianello, *J. Electroanal. Chem.* **1996**, *418*, 47–52.

[36] B. A. Sim, P. H. Milne, D. Griller, D. D. M. Wayner, *J. Am. Chem. Soc.* **1990**, *112*, 6635–6638.

[37] H. Kojima, A. J. Bard, *J. Am. Chem.* Soc. **1975**, *97*, 6317–6324.

[38] The $\Delta G_0^{\neq}$ values were calculated from: C. P. Andrieux, C. Blocman, J.-M. Dumas-Bouchiat, J.-M. Savéant, *J. Am. Chem. Soc.* **1979**, *101*, 3431–3441.

[39] T. B. Christensen, K. Daasbjerg, *Acta. Chem. Scand.* **1997**, *51*, 307–317.

[40] The $\Delta G_{0\,hom}^{\neq}$ values were calculated from: A. A. Isse, A. Gennaro, *J. Phys. Chem. A* **2004**, *108*, 4180–4186.

[41] a) C. P. Andrieux, I. Gallardo, J.-M. Savéant, K.-B. Su, *J. Am. Chem. Soc.* **1986**, *108*, 638–647; b) J.-M. Savéant, *J. Am. Chem. Soc.* **1992**, *114*, 10595–10602.

[42] The $(\Delta G_0^{\neq})_{hom}$ values were calculated from: a) K. Daasbjerg, H. Lund, *Acta Chem. Scand.* **1993**, 597–604; b) Y. Huang, D. D. M. Wayner, *J. Am. Chem. Soc.* **1994**, *116*, 2157–2158.

[43] The $(\Delta G_0^{\neq})_{hom}$ values were calculated[41b] from: T. Lund, H. Lund, *Acta Chem. Scand.* **1987**, *41*, 93–102.

[44] C. P. Andrieux, L. Gélis, M. Medebielle, J. Pinson, J.-M. Savéant, *J. Am. Chem. Soc.* **1990**, *112*, 3509–3520.

[45] R. L. Donkers, M. S. Workentin, *Chem. Eur. J.* **2001**, *7*, 4012–4020.

[46] S. Antonello, M. Crisma, F. Formaggio, A. Moretto, F. Taddei, C. Toniolo, F. Maran, *J. Am. Chem. Soc.* **2003**, *125*, 11503–11513.

[47] Inclusion of the double-layer correction for the heterogeneous data or using the E° obtained from redox catalysis measurements does not change the trend appreciably, also because the comparison concerns a very extended range of $\Delta G_0^{\neq}$ values.

[48] a) R. A. Marcus, *J. Chem. Phys.* **1956**, *24*, 966–978; b) R. A. Marcus, *J. Chem. Phys.* **1965**, *43*, 679–701.

Received: March 8, 2007
Published online: July 6, 2007

